ACS Catalysis

pubs.acs.org/acscatalysis Research Article

Tuning the Catalytic Activity of Fe-Phthalocyanine-Based Catalysts for the Oxygen Reduction Reaction by Ligand Functionalization

Shuai Yuan, Jiayu Peng, Yirui Zhang, Daniel J. Zheng, Sujay Bagi, Tao Wang, Yuriy Román-Leshkov,* and Yang Shao-Horn*

Cite This: *ACS Catal.* 2022, 12, 7278–7287 Read Online

ACCESS | Metrics & More | Article Recommendations | Supporting Information

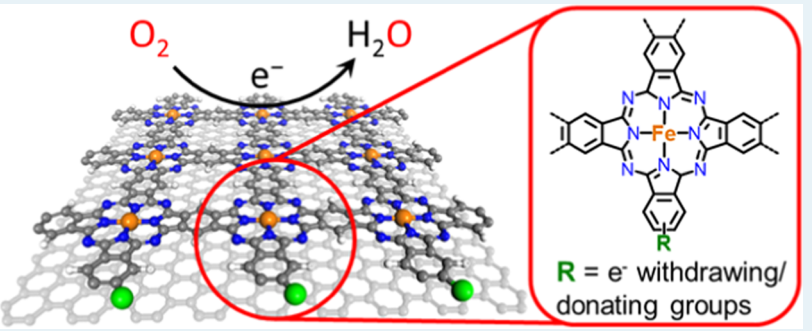

ABSTRACT: Catalysts based on Fe-N_x sites have promising catalytic activity for the oxygen reduction reaction (ORR). While homogeneous Fe-N_4 macrocycle molecules and heterogeneous Fe-N-doped carbon materials have been studied extensively, systematic strategies to tune the ORR energetics and activities of Fe-N_x-based catalytic sites remain elusive. Herein, we show that carbon-supported Fe-phthalocyanine-based catalysts (FePPc/C) can be functionalized by electron-withdrawing/donating substituents to tune the electronic structures of the Fe center and the ORR catalytic activity. FePPc/C was synthesized via the polymerization of $FeSO_4$, pyromellitic diimide, and urea on acid-treated acetylene black. By partially replacing the bridging pyromellitic diimide with terminal phthalimide bearing different functional groups (-R), functionalized Fe-phthalocyanine-based catalysts (FePPc-R/C) were obtained with -R anchoring on the edge of the polymer. Notably, the $Fe^{2+/3+}$ redox potential of Fe sites from FePPc-R/C was shifted by 0.35 V via different functional groups, where increasing redox potential was correlated with greater Hammett constants (i.e., stronger electron-withdrawing) of functional groups. Moreover, the specific and mass ORR activity of FePPc-R/C in 0.1 M $HClO_4$ could be increased by up to 20 times with increasing electron-withdrawing functional groups, where a linear relationship was observed between the $Fe^{2+/3+}$ redox potential and ORR activity, with dicarboxylate-functionalized FePPc-$(COOH)_2$/C showing the highest activity. This versatile method can be used to further design M-N_4-based catalysts for ORR and beyond.

KEYWORDS: *oxygen reduction reaction, Fe-phthalocyanine, Fe-N_4 center, redox potential, electronic tuning*

1. INTRODUCTION

The sluggish kinetics of the oxygen reduction reaction (ORR) represent a critical bottleneck in the development of fuel cells.[1−5] For example, proton-exchange membrane fuel cells (PEMFCs) use Pt alloys[2,4,6−10] to accelerate the ORR kinetics in acids, but their high price and low reserve can hinder their applications at scale. Recent studies have been focusing on nonprecious-metal-based ORR catalysts, including transition-metal nitrides,[11,12] M-N_4 macrocycle complexes,[13] and M-N-doped carbon (M-N-C) materials,[14−17] where M-N-C-based catalysts with M-N_4 centers[18,19] are one of the most promising candidates to replace Pt-based alloys to catalyze ORR in acids.

M-N_4 macrocycles have been widely studied as ORR catalysts.[13,20] For example, the Fe-porphyrin molecule in cytochrome c oxidase is a naturally occurring ORR catalyst.[21] Artificial catalysts with M-N_4 macrocycles such as metal phthalocyanine (MPc) have been studied as ORR catalysts in alkaline fuel cells since 1964.[13] Later, MPc catalysts with different metal centers (M = Fe, Co, Mn, Cr, Ni, Cu, and Zn)[22,23] and variable functional groups[20,24,25] have been examined to catalyze ORR in bases. For instance, Zagal and co-workers have reported that the ORR activity of MPcs can be manipulated by adjusting the $M^{2+/3+}$ redox potential via the

Received: January 11, 2022
Revised: April 9, 2022

https://doi.org/10.1021/acscatal.2c00184
ACS Catal. 2022, 12, 7278−7287

replacement of metal centers (M = Fe, Co, Mn, and Cr)[22] and the introduction of electron-donating/withdrawing groups.[24,25] A volcano relationship has been observed between the ORR activity and $M^{2+/3+}$ redox potential of MPcs in bases, where Fe, Mn, and CrPcs are located on the strong oxygen-binding side (with rate-limiting *OH desorption to generate OH^-) and CoPc is on the weak binding side (with rate-limiting O_2 adsorption to generate *OOH).[25] Despite their tunability and high activity under alkaline conditions, the practical applications of FePc-based catalysts in PEMFCs have been limited by their low stability,[26] where FePc undergoes demetallation in acids under ORR potential, as revealed by operando infrared (IR)[27] and Raman[28] spectroscopic studies.

Converting homogeneous FePc catalysts into heterogeneous M-N-C-based materials has been shown to enhance the stability during ORR.[29−31] These M-N-C catalysts can be synthesized usually by pyrolyzing carbon-supported MPc molecules or other M-N-complexes at high temperatures (600−1100 °C).[15,29−33] This pyrolysis process breaks the macrocyclic structure while transferring the $M-N_4$ sites into the carbon matrix.[34] The facile pyrolysis method has triggered a surge of M-N-C catalysts with enhanced ORR catalytic activity[30,33,35] ($E_{1/2}$ = 0.85 V_{RHE} with 800 $\mu g\ cm_{geo.}^{-2}$ catalyst loading[33]) and stability[17,33] (stable for 10,000 potential cycles between 0.6 and 1.0 V_{RHE} in 0.5 M H_2SO_4[33]) compared with molecular FePcs.[27] Such M-N-C catalysts have been applied in PEMFCs, achieving activity approaching state-of-the-art Pt catalysts (0.4 mg cm^{-2} Pt at a cell voltage of ≥0.9 V).[14,30,35,36] However, the high synthetic temperature complicates the characterization of active centers[37] and removes the organic functional groups that could regulate the electronic structure and catalytic activity of metal centers. These challenges limit the understanding of the ORR mechanism[16] and hinder further rational designs of catalytic activity by tuning the coordination environments of active sites. Therefore, synthetic methods are needed to control the structure and activity of $M-N_4$ catalytic centers within the heterogeneous M-N-C catalysts.

Polymerization of FePc on the surface of carbon supports allows the synthesis of heterogeneous Fe-N-C catalysts with tunability comparable to that of molecular FePcs.[38] For example, Fe-phthalocyanine-polymers (FePPc) have been synthesized on carbon supports (FePPc/C), which show high activity ($E_{1/2}$ = 0.80 V) and stability in acids (stable for 5000 potential cycles between 0.6 and 1.0 V_{RHE} in 0.5 M H_2SO_4),[39] comparable to that of Fe-N-C catalysts synthesized by pyrolysis.[33] Considering that the Fe sites are separated from aggregation in FePPc/C,[40] the material is expected to have homogeneously dispersed Fe active sites within a heterogeneous platform. More importantly, the low polymerization temperature (<400 °C) ensures the intactness of organic functional groups, which opens opportunities for further modification of FePPc/C catalysts via organic substitution. Incorporating functional groups with different electron-withdrawing/donating properties is expected to modulate the electronic structures of the Fe catalytic center in heterogeneous FePPc/C catalysts, analogous to the modulation of molecular FePc catalysts.[24,25] The resulting materials have the potential to achieve high activity by molecular design while maintaining the stability of heterogeneous catalysts. To achieve this goal, functionalized FePPc/C materials (namely, FePPc-R/C) have been synthesized by the polymerization of pyromellitic diimide, functionalized phthalimide, and urea on acid-treated acetylene black with a series of different electron-withdrawing/donating functional groups, including amino ($-NH_2$), methoxyl (−OMe), methyl (−Me), −H, carboxylic acid (−COOH), nitro ($-NO_2$), dicarboxylic acid ($-(COOH)_2$), tetrachloro ($-Cl_4$), and pyridyl (−py) groups. Importantly, the modification of FePPc-R/C by electron-withdrawing groups shifts the $Fe^{2+/3+}$ redox to a lower potential, where the redox peak shift is correlated with the Hammett constant of incorporated functional groups. We further correlate the ORR activity with the $Fe^{2+/3+}$ redox potential, exhibiting a linear relationship. The optimized catalyst, FePPc-$(COOH)_2$/C, has a half-wave potential of 0.80 V_{RHE} in 0.1 M $HClO_4$ at a loading of 500 $\mu g\ cm_{geo.}^{-2}$ and retained 73% of current density at 0.70 V_{RHE} at 1600 rpm in O_2-saturated $HClO_4$ after continuous operation at 0.6 V_{RHE} for 5 h.

2. RESULTS AND DISCUSSION

2.1. Synthesis and Functionalization of Fe-Phthalocyanine Polymers on Carbon. The Fe-phthalocyanine polymer on carbon was synthesized by reacting $FeSO_4$, pyromellitic diimide, urea, and acid-treated acetylene black, with sodium molybdate serving as the catalyst. In previous studies, pyromellitic dianhydride has been generally adopted as the precursor to synthesize MPPcs.[38,41,42] In this work, we replace pyromellitic dianhydride with pyromellitic diimide for the following reasons. First, pyromellitic diimide is expected to coordinate with metal cations in the reaction precursor,[43] which avoids the aggregation of Fe species. Second, pyromellitic diimide is known to interact more strongly with carbon supports than pyromellitic dianhydride,[44] allowing for the strong adsorption and uniform distribution of pyromellitic diimide on carbon supports. Third, the imide is known as the reaction intermediate during the synthesis of metal phthalocyanine from anhydride precursors.[45] Thus, the use of pyromellitic diimide may shorten the reaction time and reduce the synthetic temperature. Herein, FePPc/C was synthesized successfully from the pyromellitic diimide precursor at 180 °C for 6 h.

The amount of carbon was tuned to achieve different FePPc loadings on the carbon support. The loading of Fe in FePPc/C was determined by inductively coupled plasma-optical emission spectrometry (ICP-OES) analysis of digested samples (Supporting Information, Experimental Details), while the weight ratio of organic phthalocyanine polymers, PPc, was quantified by thermogravimetric analysis (TGA, Table S1). The weight loss at 380 and 550 °C is attributed to the decomposition of PPc and carbon species, respectively, from which the weight percent of PPc was calculated (Figure S1). As the amount of carbon increases from 25 mg to 200 mg, the weight loss of FePPc/C at 380 °C decreases from 62.9 to 26.2%, indicating a reduced FePPc loading. The Fe-to-PPc weight ratio in all FePPc/C products was estimated to be 0.16, which is consistent with the formula of FePPc, $[Fe-(C_{10}N_4H_2)_2]_n$. The BET surface area of FePPc/C, measured by N_2 adsorption isotherms at 77 K, was found to decrease with higher FePPc loading on carbon (Figure S2). This result indicates that FePPc may occupy the pores of carbon supports. The electrochemically accessible Fe sites were estimated by integrating the Coulombic charge of $Fe^{2+/3+}$ redox peaks in cyclic voltammograms (CV). The amount of electrochemically accessible Fe sites increases from 22 to 36 mmol g^{-1} as the Fe loading increases from 3.5 to 7.0 wt % (Figure S3). Further increasing the Fe loading to 10.1 wt % caused a significant decrease in electrochemically accessible Fe sites to 0.2 mmol

https://doi.org/10.1021/acscatal.2c00184
ACS Catal. 2022, 12, 7278−7287

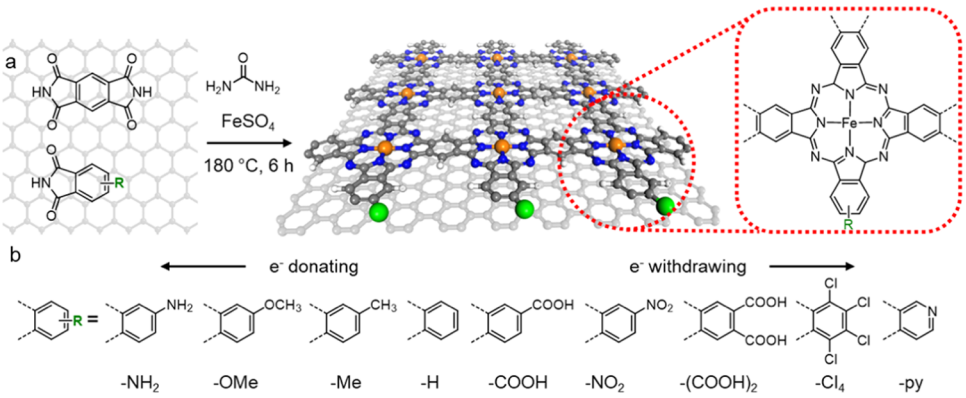

Figure 1. (a) Synthesis of FePPc-R/C by reacting a solid mixture of pyromellitic diimide, functionalized phthalimide, $FeSO_4$, and urea in a sealed glass vial at 180 °C for 6 h. The inset shows the proposed local structure of the Fe center with functional groups placed on the edge of the phenyl ring. (b) List of functional groups in FePPc-R/C with different electron-withdrawing/donating effects, including $-NH_2$, −OMe, −Me, −H, −COOH, $-NO_2$, $-(COOH)_2$, $-Cl_4$, and −py groups.

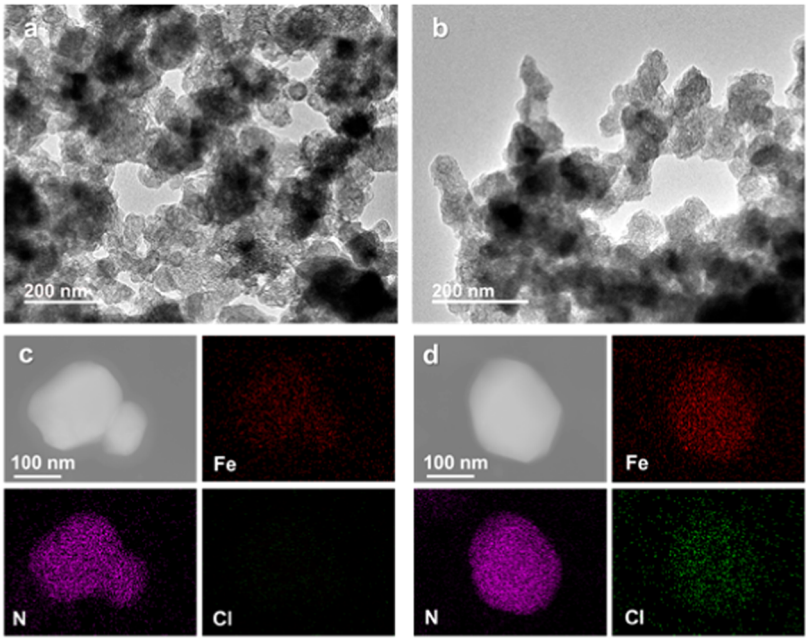

Figure 2. TEM images of (a) FePPc-$(COOH)_2$/C and (b) FePPc-Cl_4/C. EDX-based elemental mapping of (c) FePPc-$(COOH)_2$/C and (d) FePPc-Cl_4/C, showing uniform distributions of elements throughout the particle.

g^{-1}, indicating that an excessive amount of FePPc may block the pores of carbon, leading to inaccessible Fe sites. Therefore, to maximize the electrochemically accessible Fe sites, the Fe loading was controlled to 7.0 wt % when 100 mg of carbon was added during the synthesis.

The complete reaction of pyromellitic diimide was confirmed by the IR spectra, in which the C═O stretch peak from imide groups at 1773 cm^{-1} was absent (Figure S4). The broad band centered at 1730 cm^{-1} (Figure S4) can be attributed to the C═O stretching in carboxylic groups either on the peripheral position of the FePPc or the acid-treated carbon support, consistent with the notion that the as-synthesized FePPc/C is terminated by a pair of carboxylic groups on the edge, possibly generated by the hydrolysis of imide groups.[42] Therefore, the as-synthesized material was termed FePPc-$(COOH)_2$/C in a later discussion.

To functionalize FePPc/C with other substituents, the pyromellitic diimide precursor was partially replaced by terminal phthalimide bearing different functional groups during the synthesis (Figure 1a). Following the previous method that bridging pyromellitic dianhydride and terminal phthalic anhydride precursors can be copolymerized into FePPc with edges terminated by phenyl groups,[42] we functionalized FePPc/C by placing different substituents on phthalimide precursors. The synthesis of functionalized FePPc/C (FePPc-R/C) was conducted by varying the diimide-to-imide ratio in precursors, while the total amount of imide moieties was maintained constant. Taking FePPc-H/C as an example, the ratio between phthalimide (PI) and pyromellitic diimide (PDI) was adjusted from 0 to 1.31, while the moles of imide moiety (i.e., PDI *2 + PI) in the precursor was maintained at 1.16 mmol (Table S2). The polymerization reaction was conducted under the same condition as that of FePPc/C, and the product was thoroughly washed with DMF to remove any molecular FePc species. With the PI/PDI ratio below 0.5, the FePPc-H weight loading on carbon was maintained (Figure S5). Further increasing the PI/PDI ratio caused a significant decrease of FePPc-H loading in the

https://doi.org/10.1021/acscatal.2c00184
ACS Catal. 2022, 12, 7278−7287

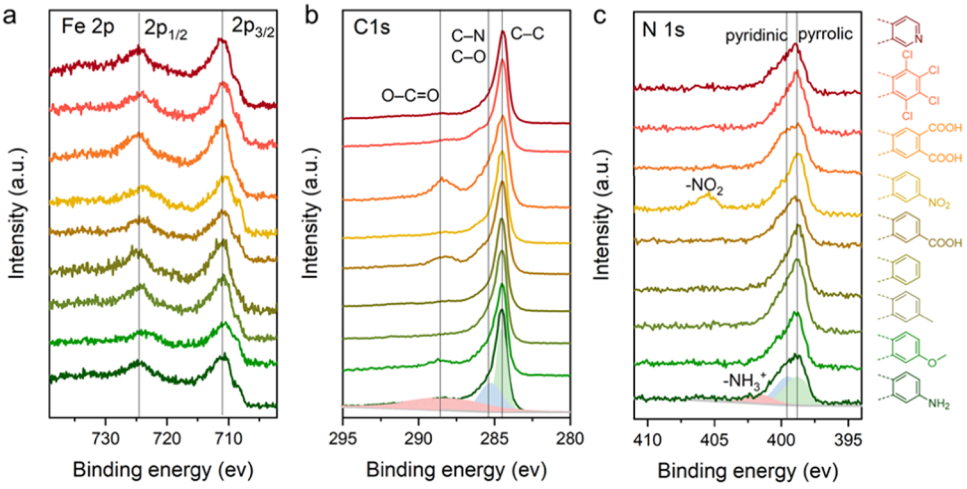

Figure 3. X-ray photoelectron spectroscopy (XPS) measurements of FePPc-R/C. (a) Fe 2p binding energy region showing Fe^{3+} with a similar coordination environment across FePPc-R/C. (b) C 1s binding region showing the existence of C−C, C−N, C−O, and O−C═O species. (c) N 1s binding energy region confirming the existence of pyridinic and pyrrolic nitrogen atoms in the Pc moieties.

products, possibly due to the formation of molecular FePc species soluble in DMF (Figure S6). The PI/PDI ratio was optimized to 0.5 to achieve maximum terminal ligand incorporation while maintaining the FePPc-H loading on the carbon support. Using functionalized phthalimide as precursors and the imide/diimide of 0.5, a series of functionalized FePPc/C were synthesized successfully (Figure 1b), namely, FePPc-R/C (R = $-NH_2$, −OMe, −Me, −H, −COOH, $-NO_2$, $-Cl_4$, and −py). Powder X-ray diffraction (PXRD) patterns of FePPc/C materials were dominated by the (002) peak of the acetylene black carbon support (Figure S7), indicating the amorphous nature of FePPc-R.

The morphology of FePPc-R/C (R = $-(COOH)_2$ and $-Cl_4$) was examined by transmission electron microscopy (TEM). TEM images show a uniform distribution of FePPc-R on the surface of acetylene black particles with an average particle size of ∼50 nm (Figures 2a,b, and S8). No aggregation of Fe species was observed. High resolution-TEM (HR-TEM) of FePPc-$(COOH)_2$/C (Figure S8b) further confirmed the isolated Fe sites without aggregation. Since FePPc-R/C with different functional groups were synthesized under similar conditions, we believe that the Fe-based nanoparticles were not formed during the synthesis of FePPc-R/C materials. The ability of FePPc/C in stabilizing high-concentration single Fe sites can be attributed to the low synthetic temperature (180 °C) and well-separated phthalocyanine chelating sites that prevent Fe aggregation.[39,40] Elemental mapping by TEM with energy-dispersive X-ray analysis (EDX) further demonstrated the uniform distribution of Fe and N species in the particle, which is in agreement with the monodispersed Fe-N_x centers in the phthalocyanine−polymer framework (Figure 2c). Moreover, the Cl signals were found to overlap well with Fe and N species under elemental mapping (Figure 2d), suggesting that the functional groups on the terminal phthalimide precursors were incorporated homogeneously in FePPc-Cl/C.

Further insights into the electronic structure of FePPc-R/C were provided by XPS. The Fe $2p_{3/2}$ and $2p_{1/2}$ peaks were located at 710.8 and 724.4 eV, respectively, corresponding to trivalent Fe (Figure 3a). Although the Fe^{2+} precursor was adopted in the synthesis, the Fe^{2+} species can be oxidized during the synthesis of FePPc/C, which agrees with previous work.[39,41,42] The incorporation of functional groups does not significantly change the Fe 2p peak positions (Figure 3a), indicating similar oxidation states and coordination environments across all materials. The C 1s spectrum was deconvoluted into three peaks corresponding to carbon species in different chemical environments (Figure 3b). The C−C peak at 284.5 eV corresponds to the sp^2 carbon in the graphite carbon support and phenyl rings of FePPc.[46,47] The C−N or C−O carbon at 285.4 eV can be assigned to the N-heterocycle of the Pc moiety or the oxygen species from acid-treated acetylene black.[47] The O−C═O peak at 288.5 eV was attributed to carboxylic acids[48] either on the peripheral position of FePPc or on the surface of the acid-treated acetylene black.[49] The dicarboxylate- and monocarboxylate-functionalized samples, FePPc-$(COOH)_2$/C and FePPc-COOH/C, show higher intensities of O−C═O peaks than other samples, in line with higher concentrations of carboxylic acids (Figure S9a). In addition, the pyridinic (399.5 eV) and pyrrolic (398.8 eV) nitrogen atoms in the Pc moiety[47,50] were observed unambiguously in the N 1s XPS spectra of all FePPc-R/C samples (Figure 3c). Moreover, the peak at 401.6 eV for FePPc-NH_2/C was attributed to the $-NH_2$ groups,[48] and the pronounced absorption peak at 405.6 eV in the N 1s spectrum of the FePPc-NO_2/C sample confirmed the existence of $-NO_2$ functional groups (Figure 3c).[51] Lastly, the organic -Cl was detected by the Cl $2p_{3/2}$ and $2p_{1/2}$ peaks at 200.4 and 202.1 eV, respectively (Figure S9b), matching previous reports.[51] The NH_2/Fe, NO_2/Fe, and Cl/Fe ratios were calculated to be 0.77, 0.82, and 3.2 based on XPS, corresponding to ∼0.8 functional ligands ($-NH_2$, $-NO_2$, and $-Cl_4$) per Fe center. The $N_{pyridinic}$/Fe of FePPc-R/C (ranging from 3.5 to 4.6, Table S3) supports the proposed FePPc structure. The $N_{pyrrolic}$/Fe ratio (ranging from 4.3 to 5.4, Table S3) is slightly higher than the $N_{pyridinic}$/Fe ratio, indicating that pyrrolic nitrogen atoms may exist in the FePc center and the N-doped carbon support. Overall, the comparable peak positions in Fe 2p and N 1s XPS spectra (Figure 3) support that all FePPc-R/C materials contain similar Fe-N_x centers. The valence band edge of all materials approaches 0 eV as estimated by XPS (Figure S9c), which can be explained by the fact that the valence band edge region of XPS is predominated by the conductive carbon supports.

https://doi.org/10.1021/acscatal.2c00184
ACS Catal. 2022, 12, 7278−7287

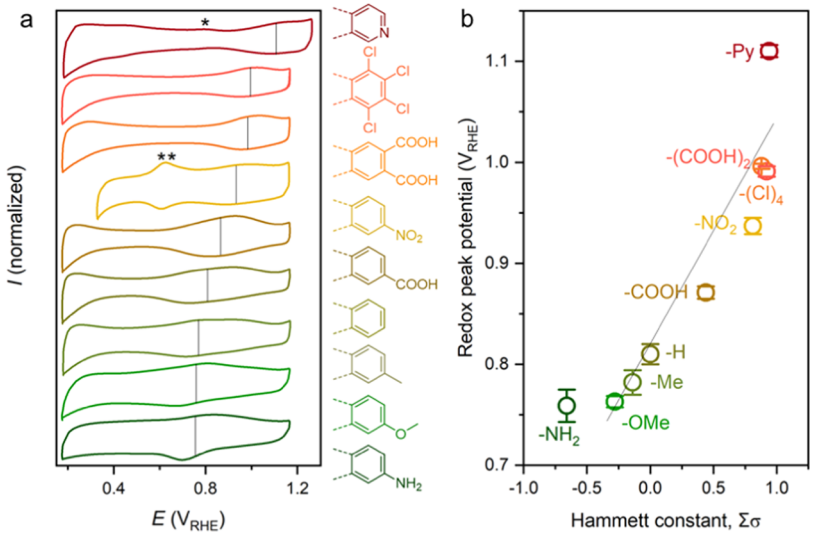

Figure 4. (a) CVs of FePPc-R/C with different functional groups. CVs were conducted in Ar-saturated 0.1 M $HClO_4$ at 10 mV s^{-1} using electrodes composed of 500 $\mu g_{cat.}$ $cm_{geo.}^{-2}$ and a Pt wire counter electrode. (b) Redox potential of FePPc-R/C determined from CVs as a function of the Hammett constant of functional groups.[53] FePPc-py/C exhibited an additional redox peak (*) at 0.75 V_{RHE} attributable to the pyridyl-coordinated Fe, which decreased with time (Figure S10), indicating the leaching of weakly coordinated Fe at pyridyl sites. FePPc-NO_2/C shows an additional peak (**) at 0.61 V_{RHE}, which can be explained by the reversible redox of $-NO_2/-NO$ groups.[57] Error bars represent the standard deviations of at least three independent measurements.

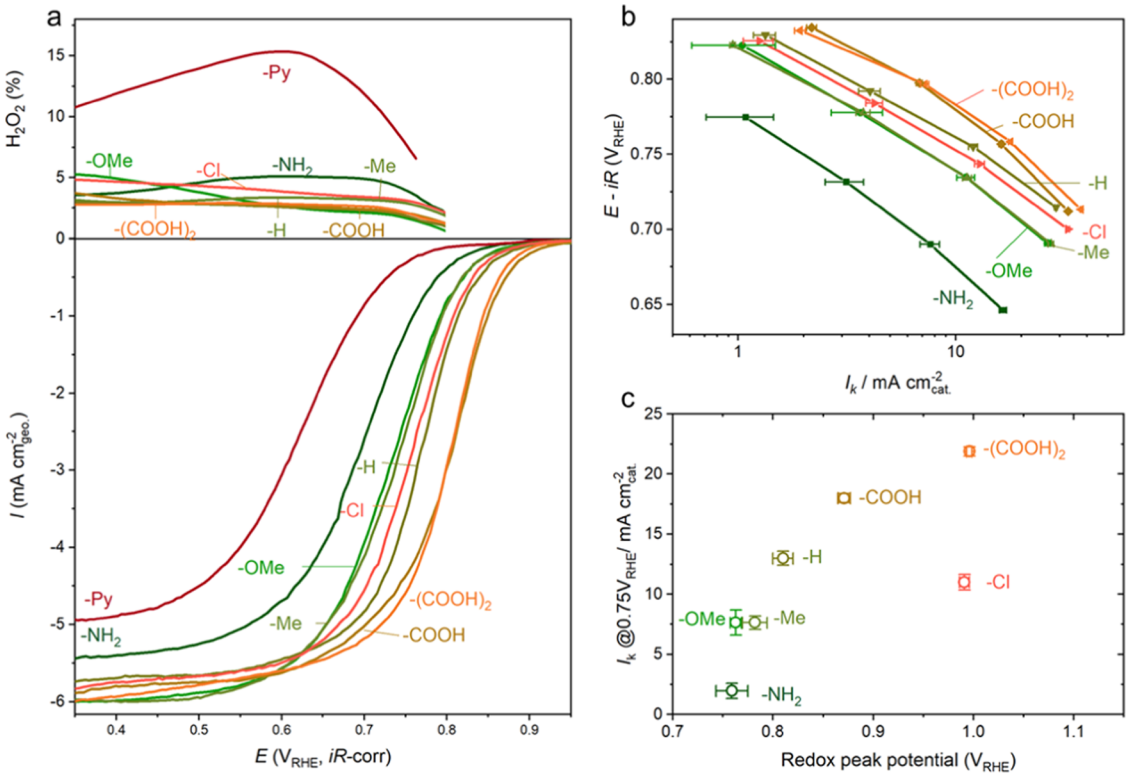

Figure 5. ORR activity of FePPc-R/C. (a) Polarization curves of FePPc-$(COOH)_2$/C measured using a thin-film electrode composed of 500 μg $cm_{geo.}^{-2}$ catalyst and a Pt wire counter electrode in O_2-saturated 0.1 M $HClO_4$ at a rotation rate of 1600 rpm and a scan rate of 10 mV s^{-1} after *iR* correction. The top figure shows the H_2O_2 yield of FePPc-R/C measured by RRDE. The electron transfer number of FePPc-$(COOH)_2$/C measured by RRDE (3.9) matched well with the calculation based on the Koutecky–Levich plot derived from polarization curves at different rotation speeds (3.9, Figure S16). (b) Tafel plots derived from CVs with mass transport corrected by the Koutecky–Levich equation (Experimental Details of the Supporting Information). The electrochemical surface area was estimated by the double-layer capacitance (Table S4). (c) Correlation between surface-specific kinetic current density at 0.75 V_{RHE} and the $Fe^{2+/3+}$ redox peak potential. Error bars were obtained from standard deviation based on at least three independent measurements.

2.2. Regulating the Redox Potential of the Fe Center by Functional Groups in FePPc-R/C. The effect of functional groups on the electronic structure and redox of the Fe center of FePPc-R/C (R = $-NH_2$, $-OMe$, $-Me$, $-H$,

https://doi.org/10.1021/acscatal.2c00184
ACS Catal. 2022, 12, 7278−7287

−COOH, $-NO_2$, $-Cl_4$, and −py) was studied by cyclic voltammetry. All FePPc-R/C materials exhibit a pair of reversible redox peaks located from 0.76 to 1.11 V_{RHE}, which can be assigned to the $Fe^{2+/3+}$ redox process of the Fe-N_x center (Figure 4a). While XPS showed no significant shifts in Fe 2p peaks (Figure 3c), possibly due to the broad Fe 2p peaks (full width at half maximum of ∼4 eV),[52] the redox potential of $Fe^{2+/3+}$ was found to be different. Electron-withdrawing groups were found to increase the $Fe^{2+/3+}$ redox potential, while electron-donating groups decreased the potential of the $Fe^{2+/3+}$ redox. The $Fe^{2+/3+}$ redox potential was found to increase linearly with greater Hammett constants (i.e., stronger electron-withdrawing effects) of functional groups with the order of $-NH_2$ < −OMe < −Me < −H < −COOH < $-NO_2$ < $-Cl_4$ = $-(COOH)_2$ < −py (Figure 4b).[53] This trend could be explained by the inductive effect of electron-withdrawing groups that decreased the electron density and stabilized the d-frontier orbital of Fe centers to favor their oxidation process.[24,54] A trend similar to that in Figure 4b has been observed in MPcs (M = Fe and Co) with different substituents attached to the molecular Pc macrocycles.[25] Herein, we compare the redox peak shift of our FePPc-R/C with FePcs and Fe-N-C materials synthesized by pyrolysis. While the redox potential shift of $Fe^{2+/3+}$ in molecular FePcs can be highly tunable (up to 0.5 V induced by different functional groups),[55] the tunability of Fe centers in the heterogeneous Fe-N-C catalyst is quite limited (<0.1 V).[16,56] The FePPc-R/C synthesized in this work allows the $Fe^{2+/3+}$ redox potential to be modulated in a wide range (up to 0.35 V), which is much higher than traditional heterogeneous Fe-N-C catalysts. The effective shift of redox peaks enabled by FePPc-R/C samples can be attributed to the uniform distribution of functionalized ligands around the Fe center, which allows the electronic tuning of the Fe center similar to molecular FePcs. On the other hand, the lack of tunability of traditional heterogeneous Fe-N-C catalysts synthesized by pyrolysis can be explained by the removal of functional groups during high-temperature synthesis (600−1100 °C).[15,29−33]

The $Fe^{2+/3+}$ redox potential of heterogeneous FePPc-H/C (0.82 V_{RHE}) was found to be higher than that of molecular FePc-H with the same −H terminated edges (0.65 V_{RHE}).[58] The higher redox potential of FePPc-H/C can be explained by the electron-withdrawing effect of neighboring Fe centers through the conjugated FePPc polymers, which is supported by DFT calculations showing that FePPc has more electron-deficient Fe centers than molecular FePc.[59] The strong interaction between the oxidized carbon support and FePPc layers may also contribute to the positive shift of the $Fe^{2+/3+}$ redox potential.[60] As the increase in the experimental $Fe^{2+/3+}$ redox potential of FePc-R catalysts was shown to decrease the binding energy of oxygen, which leads to increasing ORR activity on metal centers,[54] the FePPc-H/C catalyst is expected to have greater ORR activity than FePc-H with the same functional group. Furthermore, the ORR activity of FePPc-R/C materials can be optimized by different functional groups.

2.3. Tuning the ORR Activity of FePPc-R/C. The ORR activity was measured by CV using a thin-film electrode consisting of 500 $\mu g\ cm_{geo.}^{-2}$ FePPc-R/C and 100 $\mu g\ cm_{geo.}^{-2}$ Nafion on a glassy carbon electrode (GCE) in O_2-saturated 0.1 M $HClO_4$ at a rotation speed of 1600 rpm.[61] ORR polarization curves for FePPc-R/C (R = $-NH_2$, −OMe, −Me, −H, −COOH, $-(COOH)_2$, $-Cl_4$, and −py) show the effect of functional groups on the ORR activity (Figure 5a). The most active catalyst, FePPc-$(COOH)_2$/C, features a $E_{1/2}$ of 0.80 V_{RHE} at a catalyst loading of 500 $\mu g\ cm_{geo.}^{-2}$, which is only slightly lower than the state-of-the-art Fe-N-C catalysts ($E_{1/2}$ = 0.85 V_{RHE} with 800 $\mu g\ cm_{geo.}^{-2}$ catalyst loading in 0.5 M H_2SO_4).[15,29−33] To rule out the impact of the Pt counter electrode on the ORR activity,[62] control experiments were conducted by measuring polarization curves of FePPc-$(COOH)_2$/C with Pt wire or carbon paper counter electrodes, which gave comparable results (Figure S11). These results are consistent with our observation that ICP-OES of the FePPc-$(COOH)_2$/C electrode and electrolyte did not detect Pt species within the detection limit (0.1 ppm, Table S5), suggesting that the counter electrode has minimal effects on the ORR activity in our measurements. The selectivity and electron transfer numbers of FePPc-R/C were measured by the rotating ring-disk electrode (RRDE) with the FePPc-R/C working electrode to reduce O_2 and the Pt ring electrode to detect generated H_2O_2. FePPc-R/C catalysts with $-NH_2$, −OMe, −Me, −H, −COOH, $-(COOH)_2$, and $-Cl_4$ functional groups show comparable low H_2O_2 yield of ∼5%, in contrast to the pyridyl-functionalized FePPc-py/C with higher H_2O_2 yield ranging from 7 to 15%. Therefore, FePPc-R/C catalysts with different functional groups mainly catalyze $4e^-$ ORR (number of electrons transferred during ORR, n = 3.9), except for FePPc-py/C, which catalyzes both $2e^-$ and $4e^-$ ORR (n = 3.75). The higher H_2O_2 yield of FePPc-py/C can be attributed to its electron-deficient Fe center promoting the 2-electron transfer pathway, which is associated with the lower ORR activity of FePPc-py/C ($E_{1/2}$ = 0.63 V_{RHE}) than those of $4e^-$ ORR catalysts. Electron-deficient sites with weak binding of oxygenated intermediates are reported to impede the *OOH to *O conversion ($4e^-$ reduction pathway involving * + O_2 + H^+ + e^- → *OOH; *OOH + H^+ + e^- → *O + H_2O; *O + H^+ + e^- → *OH; *OH + H^+ + e^- → * + H_2O) and thus favor the *OOH to H_2O_2 conversion ($2e^-$ reduction pathway involving * + O_2 + H^+ + e^- → *OOH; *OOH + H^+ + e^- → * + H_2O_2, Figure S12).[25,41,54] It should be noted that the apparent H_2O_2 yield by RRDE can be dependent on the catalyst loading, which has been shown previously.[63−65] This trend was also found for the FePPc-R/C catalyst, where the detected H_2O_2 slightly increased from 2.5 to 3.5% as the FePPc-$(COOH)_2$/C loading decreased from 750 to 250 $\mu g\ cm_{geo.}^{-2}$ (Figure S13). Similarly, the apparent H_2O_2 yield of FePPc-NH_2/C increased from 3.3 to 5.7% as the loading reduced from 750 to 250 $\mu g\ cm_{geo.}^{-2}$ (Figure S14). While the H_2O_2 yield slightly increased as the loading decreased, the H_2O_2 yield was still less than 5.7% at a low loading of 250 $\mu g\ cm_{geo.}^{-2}$, demonstrating that the $4e^-$ ORR pathway remains dominant for FePPc-R/C.

The activity of $4e^-$ ORR catalysts was compared, including FePPc-R/C (R = $-NH_2$, −OMe, −Me, −H, −COOH, $-(COOH)_2$, and $-Cl_4$). To eliminate the influence of mass loading, surface area differences, and mass transport limitations, the kinetic current densities were calculated from the polarization curves (in O_2-saturated 0.1 M $HClO_4$ at a rotation rate of 1600 rpm and a scan rate of 10 mV s^{-1} after iR correction) by the Koutecky−Levich equation and normalized by either the surface area or the mass loading of Fe. The resulting surface-specific activity and mass-specific activity were compared in the Tafel plots (Figures 5b and S15). The surface area-normalized kinetic current density at 0.75 V_{RHE} increases with higher $Fe^{2+/3+}$ redox peak potential (Figure 5c), suggesting that weakening the binding of oxygenated species

https://doi.org/10.1021/acscatal.2c00184
ACS Catal. 2022, 12, 7278−7287

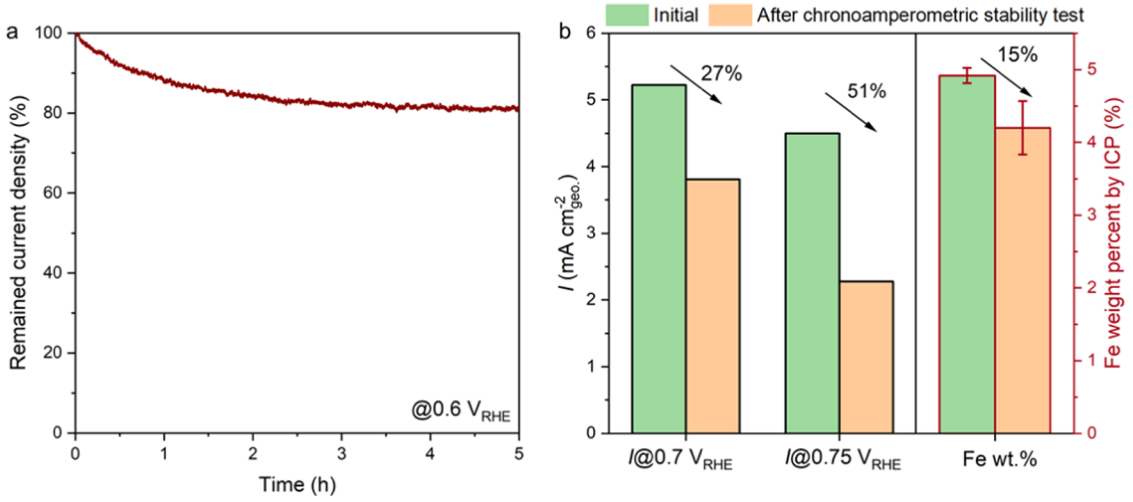

Figure 6. Stability test of FePPc-$(COOH)_2$/C. (a) Stability test by chronoamperometry using a thin-film electrode composed of 500 μg $cm_{geo.}^{-2}$ FePPc-$(COOH)_2$/C catalyst and a carbon paper counter electrode in O_2-saturated 0.1 M $HClO_4$ at 0.6 V_{RHE} for 5 h. (b) ORR activity evaluated by the current density at 0.70 and 0.75 V_{RHE} from CV measurements at 10 mV s^{-1} and 1600 rpm, and Fe wt % in FePPc-$(COOH)_2$/C measured by ICP before and after chronoamperometric stability test (0.1 M $HClO_4$ at 0.6 V_{RHE} for 5 h).

facilitates the ORR on FePPc-R/C (R = $-NH_2$, $-OMe$, $-Me$, $-H$, $-COOH$, $-(COOH)_2$, and $-Cl_4$). Given that the $Fe^{2+/3+}$ redox potential is related linearly to the Hammett constant of functional groups, the activity of FePPc-R can be rationally tuned by selecting functional groups with appropriate Hammett constants.

The most active catalyst, FePPc-$(COOH)_2$/C, was further investigated. FePPc-$(COOH)_2$/C remained stable during ORR activity tests, as revealed by the CVs before and after ORR measurements (in O_2-saturated 0.1 M $HClO_4$ at a rotation rate of 1600 rpm and a scan rate of 10 mV s^{-1} from 0.2 to 1.1 V_{RHE} for 5 cycles, Figure S17). Furthermore, the stability of FePPc-$(COOH)_2$/C was assessed by chronoamperometric tests at 0.6 V_{RHE} in O_2-saturated $HClO_4$ for 5 h (Figure 6a). After the chronoamperometric test, the current density at 0.70 and 0.75 V_{RHE} at 1600 rpm in O_2-saturated $HClO_4$ was found to decrease by 27 and 51%, respectively (Figure 6b). The H_2O_2 yield of FePPc-$(COOH)_2$/C was measured to be 6.5% after the chronoamperometric test (500 μg $cm_{geo.}^{-2}$ catalyst in 0.1 M $HClO_4$ at 0.6 V_{RHE} for 5 h) corresponding to an electron transfer number of 3.7 (Figure S18). The stability of FePPc-$(COOH)_2$/C represents a significant improvement over the molecular FePc catalyst, as FePc is known to undergo rapid deactivation under ORR conditions within 10 min in acids.[28] The higher stability of FePPc-$(COOH)_2$/C than molecular FePc can be tentatively attributed to the rigid network structure and more electron-withdrawing ligands that prevent the demetallation of FePPc and the protonation of PPc.[17] The stability of FePPc-$(COOH)_2$/C is comparable to that of the Fe-N-C catalyst synthesized by high-temperature pyrolysis.[15] Previous studies on Fe-N-C materials reveal complicated degeneration mechanisms, which possibly involve carbon corrosion,[66,67] Fe dissolution,[68] and Fe aggregation.[69,70] Therefore, we used ICP-OES, HR-TEM, and XPS experiments to study the degradation mechanisms of FePPc-$(COOH)_2$/C. ICP-OES results indicate 15% leaching of Fe from FePPc-$(COOH)_2$/C after the chronoamperometric test in O_2-saturated $HClO_4$ at 0.6 V_{RHE} for 5 h (Table S5). HR-TEM images do show the appearance of dark domains, which might indicate the aggregation of Fe species, although the lattices of Fe or Fe oxides were not observed (Figure S19). In XPS spectra, the Fe 2p peak position was not shifted after the chronoamperometric test, indicating the maintained oxidation state of Fe species (Figure S20a). In addition, the C 1s, N 1s, and O 1s signals were not significantly altered after the chronoamperometric test (Figure S20b–d), which excludes the oxidation of surface PPc or carbon species. Based on these results, we infer that the decrease of ORR current density by 25 and 51% at 0.70 and 0.75 V_{RHE}, respectively, is mainly associated with the detachment of Fe from the FePc center. This is in line with previous studies on the degradation of FePcs during ORR.[68] However, we cannot rule out the possibility of Fe aggregation or coordination environment change causing an activity change, which requires further studies by Mössbauer or Fe K-edge extended X-ray absorption fine structure (EXAFS) spectra.

3. CONCLUSIONS

In conclusion, we report a series of FePPc-R/C with functional groups providing electronically tunable Fe centers. The relatively low synthetic temperature ensures the intactness of functional groups within FePPc-R/C, which is in sharp contrast to the Fe-N-C materials synthesized by high-temperature pyrolysis. The redox potential of FePPc-R/C has been modulated over a wide range (up to 0.35 V), demonstrating a significantly higher tunability than traditional heterogeneous Fe-N-C catalysts. The Hammett constant has been used as a descriptor of the electronic structure and ORR activity of FePPc-R/C. The optimized catalyst, FePPc-$(COOH)_2$/C, achieves high activity ($E_{1/2}$ = 0.80 V_{RHE} in 0.1 M $HClO_4$ at a loading of 500 μg cm_{geo}^{-2}). This work has not only provided a promising precious-metal-free ORR catalyst candidate but also invented a versatile synthetic method for highly tunable heterogeneous electrocatalysts. Considering the wide applications of M-N_4-based materials in electrocatalysis, photocatalysis, and thermal catalysis, future catalysts can be rationally designed for targeted applications by selecting functional groups with appropriate Hammett constants.

https://doi.org/10.1021/acscatal.2c00184
ACS Catal. 2022, 12, 7278−7287

■ ASSOCIATED CONTENT

Supporting Information

The Supporting Information is available free of charge at https://pubs.acs.org/doi/10.1021/acscatal.2c00184.

Detailed material synthesis, electrochemical tests, PXRD, N_2 adsorption isotherms, and ICP-OES results (PDF)

■ AUTHOR INFORMATION

Corresponding Authors

Yuriy Román-Leshkov − *Department of Chemical Engineering, Massachusetts Institute of Technology, Cambridge, Massachusetts 02139, United States;* orcid.org/0000-0002-0025-4233; Email: yroman@mit.edu

Yang Shao-Horn − *Department of Mechanical Engineering, Massachusetts Institute of Technology, Cambridge, Massachusetts 02139, United States; Department of Materials Science and Engineering, Massachusetts Institute of Technology, Cambridge, Massachusetts 02139, United States;* orcid.org/0000-0001-8714-2121; Email: shaohorn@mit.edu

Authors

Shuai Yuan − *Department of Mechanical Engineering, Massachusetts Institute of Technology, Cambridge, Massachusetts 02139, United States; Department of Materials Science and Engineering, Research Laboratory of Electronics, and Department of Chemical Engineering, Massachusetts Institute of Technology, Cambridge, Massachusetts 02139, United States;* orcid.org/0000-0003-3329-0481

Jiayu Peng − *Department of Materials Science and Engineering, Massachusetts Institute of Technology, Cambridge, Massachusetts 02139, United States;* orcid.org/0000-0003-3696-770X

Yirui Zhang − *Department of Mechanical Engineering, Massachusetts Institute of Technology, Cambridge, Massachusetts 02139, United States;* orcid.org/0000-0001-7604-8623

Daniel J. Zheng − *Department of Materials Science and Engineering, Massachusetts Institute of Technology, Cambridge, Massachusetts 02139, United States*

Sujay Bagi − *Department of Chemical Engineering, Massachusetts Institute of Technology, Cambridge, Massachusetts 02139, United States*

Tao Wang − *Department of Mechanical Engineering, Massachusetts Institute of Technology, Cambridge, Massachusetts 02139, United States; Department of Materials Science and Engineering and Research Laboratory of Electronics, Massachusetts Institute of Technology, Cambridge, Massachusetts 02139, United States*

Complete contact information is available at: https://pubs.acs.org/10.1021/acscatal.2c00184

Author Contributions

Y.S-H., Y.R-L., and S.Y. conceived the original idea. S.Y. and D.J.Z. performed the synthesis. S.Y., D.J.Z., J.P., and T.W. performed the electrochemical measurements and data analysis. Y.Z. and J.P. conducted the XPS measurements. S.B. conducted the TEM measurements. S.Y., J.P., T.W., D.J.Z., Y.S-H., and Y.R-L. drafted the manuscript. All authors contributed to the revision of the manuscript.

Notes

The authors declare no competing financial interest.

■ ACKNOWLEDGMENTS

This work was supported by the Toyota Research Institute through the Accelerated Materials Design and Discovery program.

■ REFERENCES

(1) Shao, M.; Chang, Q.; Dodelet, J.-P.; Chenitz, R. Recent Advances in Electrocatalysts for Oxygen Reduction Reaction. *Chem. Rev.* **2016**, *116*, 3594−3657.

(2) Gasteiger, H. A.; Kocha, S. S.; Sompalli, B.; Wagner, F. T. Activity benchmarks and requirements for Pt, Pt-alloy, and non-Pt oxygen reduction catalysts for PEMFCs. *Appl. Catal., B* **2005**, *56*, 9−35.

(3) Nørskov, J. K.; Rossmeisl, J.; Logadottir, A.; Lindqvist, L.; Kitchin, J. R.; Bligaard, T.; Jónsson, H. Origin of the Overpotential for Oxygen Reduction at a Fuel-Cell Cathode. *J. Phys. Chem. B* **2004**, *108*, 17886−17892.

(4) Han, B.; Carlton, C. E.; Kongkanand, A.; Kukreja, R. S.; Theobald, B. R.; Gan, L.; O'Malley, R.; Strasser, P.; Wagner, F. T.; Shao-Horn, Y. Record activity and stability of dealloyed bimetallic catalysts for proton exchange membrane fuel cells. *Energy Environ. Sci.* **2015**, *8*, 258−266.

(5) Mukerjee, S.; Srinivasan, S. Enhanced electrocatalysis of oxygen reduction on platinum alloys in proton exchange membrane fuel cells. *J. Electroanal. Chem.* **1993**, *357*, 201−224.

(6) Stamenkovic, V. R.; Fowler, B.; Mun Bongjin, S.; Wang, G.; Ross Philip, N.; Lucas Christopher, A.; Marković Nenad, M. Improved Oxygen Reduction Activity on Pt3Ni(111) via Increased Surface Site Availability. *Science* **2007**, *315*, 493−497.

(7) Zhang, J.; Lima, F. H. B.; Shao, M. H.; Sasaki, K.; Wang, J. X.; Hanson, J.; Adzic, R. R. Platinum Monolayer on Nonnoble Metal−Noble Metal Core−Shell Nanoparticle Electrocatalysts for O2 Reduction. *J. Phys. Chem. B* **2005**, *109*, 22701−22704.

(8) Xu, Y.; Ruban, A. V.; Mavrikakis, M. Adsorption and Dissociation of O2 on Pt−Co and Pt−Fe Alloys. *J. Am. Chem. Soc.* **2004**, *126*, 4717−4725.

(9) Strasser, P.; Koh, S.; Anniyev, T.; Greeley, J.; More, K.; Yu, C.; Liu, Z.; Kaya, S.; Nordlund, D.; Ogasawara, H.; Toney, M. F.; Nilsson, A. Lattice-strain control of the activity in dealloyed core−shell fuel cell catalysts. *Nat. Chem.* **2010**, *2*, 454−460.

(10) Escudero-Escribano, M.; Malacrida, P.; Hansen Martin, H.; Vej-Hansen Ulrik, G.; Velázquez-Palenzuela, A.; Tripkovic, V.; Schiøtz, J.; Rossmeisl, J.; Stephens Ifan, E. L.; Chorkendorff, I. Tuning the activity of Pt alloy electrocatalysts by means of the lanthanide contraction. *Science* **2016**, *352*, 73−76.

(11) Zhong, H.; Zhang, H.; Liu, G.; Liang, Y.; Hu, J.; Yi, B. A novel non-noble electrocatalyst for PEM fuel cell based on molybdenum nitride. *Electrochem. Commun.* **2006**, *8*, 707−712.

(12) Qi, J.; Jiang, L.; Jiang, Q.; Wang, S.; Sun, G. Theoretical and Experimental Studies on the Relationship between the Structures of Molybdenum Nitrides and Their Catalytic Activities toward the Oxygen Reduction Reaction. *J. Phys. Chem. C* **2010**, *114*, 18159−18166.

(13) Jasinski, R. A new fuel cell cathode catalyst. *Nature* **1964**, *201*, 1212−1213.

(14) Wu, G.; More, K. L.; Johnston, C. M.; Zelenay, P. High-performance electrocatalysts for oxygen reduction derived from polyaniline, iron, and cobalt. *Science* **2011**, *332*, 443−447.

(15) Byon, H. R.; Suntivich, J.; Shao-Horn, Y. Graphene-Based Non-Noble-Metal Catalysts for Oxygen Reduction Reaction in Acid. *Chem. Mater.* **2011**, *23*, 3421−3428.

(16) Ramaswamy, N.; Tylus, U.; Jia, Q.; Mukerjee, S. Activity Descriptor Identification for Oxygen Reduction on Nonprecious Electrocatalysts: Linking Surface Science to Coordination Chemistry. *J. Am. Chem. Soc.* **2013**, *135*, 15443−15449.

(17) Xie, X.; He, C.; Li, B.; He, Y.; Cullen, D. A.; Wegener, E. C.; Kropf, A. J.; Martinez, U.; Cheng, Y.; Engelhard, M. H.; Bowden, M. E.; Song, M.; Lemmon, T.; Li, X. S.; Nie, Z.; Liu, J.; Myers, D. J.; Zelenay, P.; Wang, G.; Wu, G.; Ramani, V.; Shao, Y. Performance enhancement and degradation mechanism identification of a single-atom Co−N−C catalyst for proton exchange membrane fuel cells. *Nat. Catal.* **2020**, *3*, 1044−1054.
(18) Chung, H. T.; Cullen David, A.; Higgins, D.; Sneed Brian, T.; Holby Edward, F.; More Karren, L.; Zelenay, P. Direct atomic-level insight into the active sites of a high-performance PGM-free ORR catalyst. *Science* **2017**, *357*, 479−484.
(19) Kramm, U. I.; Herranz, J.; Larouche, N.; Arruda, T. M.; Lefèvre, M.; Jaouen, F.; Bogdanoff, P.; Fiechter, S.; Abs-Wurmbach, I.; Mukerjee, S.; Dodelet, J.-P. Structure of the catalytic sites in Fe/N/C-catalysts for O2-reduction in PEM fuel cells. *Phys. Chem. Chem. Phys.* **2012**, *14*, 11673−11688.
(20) Kumar, A.; Zhang, Y.; Liu, W.; Sun, X. The chemistry, recent advancements and activity descriptors for macrocycles based electrocatalysts in oxygen reduction reaction. *Coord. Chem. Rev.* **2020**, *402*, No. 213047.
(21) Tsukihara, T.; Aoyama, H.; Yamashita, E.; Tomizaki, T.; Yamaguchi, H.; Shinzawa-Itoh, K.; Nakashima, R.; Yaono, R.; Yoshikawa, S. Structures of metal sites of oxidized bovine heart cytochrome c oxidase at 2.8 A. *Science* **1995**, *269*, 1069−1074.
(22) Zagal, J.; Páez, M.; Tanaka, A. A.; dos Santos, J. R.; Linkous, C. A. Electrocatalytic activity of metal phthalocyanines for oxygen reduction. *J. Electroanal. Chem.* **1992**, *339*, 13−30.
(23) Singh, D. K.; Ganesan, V.; Yadav, D. K.; Yadav, M. Metal (Mn, Fe, Co, Ni, Cu, and Zn) Phthalocyanine-Immobilized Mesoporous Carbon Nitride Materials as Durable Electrode Modifiers for the Oxygen Reduction Reaction. *Langmuir* **2020**, *36*, 12202−12212.
(24) Zagal, J. H. Metallophthalocyanines as catalysts in electrochemical reactions. *Coord. Chem. Rev.* **1992**, *119*, 89−136.
(25) Zagal, J. H.; Koper, M. T. M. Reactivity Descriptors for the Activity of Molecular MN4 Catalysts for the Oxygen Reduction Reaction. *Angew. Chem., Int. Ed.* **2016**, *55*, 14510−14521.
(26) Baranton, S.; Coutanceau, C.; Roux, C.; Hahn, F.; Léger, J.-M. Oxygen reduction reaction in acid medium at iron phthalocyanine dispersed on high surface area carbon substrate: tolerance to methanol, stability and kinetics. *J. Electroanal. Chem.* **2005**, *577*, 223−234.
(27) Baranton, S.; Coutanceau, C.; Roux, C.; Hahn, F.; Léger, J. M. Oxygen reduction reaction in acid medium at iron phthalocyanine dispersed on high surface area carbon substrate: tolerance to methanol, stability and kinetics. *J. Electroanal. Chem.* **2005**, *577*, 223−234.
(28) Chen, Z.; Jiang, S.; Kang, G.; Nguyen, D.; Schatz, G. C.; Van Duyne, R. P. Operando Characterization of Iron Phthalocyanine Deactivation during Oxygen Reduction Reaction Using Electrochemical Tip-Enhanced Raman Spectroscopy. *J. Am. Chem. Soc.* **2019**, *141*, 15684−15692.
(29) Faubert, G.; Lalande, G.; Côté, R.; Guay, D.; Dodelet, J. P.; Weng, L. T.; Bertrand, P.; Dénès, G. Heat-treated iron and cobalt tetraphenylporphyrins adsorbed on carbon black: Physical characterization and catalytic properties of these materials for the reduction of oxygen in polymer electrolyte fuel cells. *Electrochim. Acta* **1996**, *41*, 1689−1701.
(30) Lefèvre, M.; Proietti, E.; Jaouen, F.; Dodelet, J.-P. Iron-Based Catalysts with Improved Oxygen Reduction Activity in Polymer Electrolyte Fuel Cells. *Science* **2009**, *324*, 71−74.
(31) Pylypenko, S.; Mukherjee, S.; Olson, T. S.; Atanassov, P. Non-platinum oxygen reduction electrocatalysts based on pyrolyzed transition metal macrocycles. *Electrochim. Acta* **2008**, *53*, 7875−7883.
(32) Wang, J.; Huang, Z.; Liu, W.; Chang, C.; Tang, H.; Li, Z.; Chen, W.; Jia, C.; Yao, T.; Wei, S.; Wu, Y.; Li, Y. Design of N-Coordinated Dual-Metal Sites: A Stable and Active Pt-Free Catalyst for Acidic Oxygen Reduction Reaction. *J. Am. Chem. Soc.* **2017**, *139*, 17281−17284.
(33) Zhang, H.; Hwang, S.; Wang, M.; Feng, Z.; Karakalos, S.; Luo, L.; Qiao, Z.; Xie, X.; Wang, C.; Su, D.; Shao, Y.; Wu, G. Single Atomic Iron Catalysts for Oxygen Reduction in Acidic Media: Particle Size Control and Thermal Activation. *J. Am. Chem. Soc.* **2017**, *139*, 14143−14149.
(34) Miller, H. A.; Bellini, M.; Oberhauser, W.; Deng, X.; Chen, H.; He, Q.; Passaponti, M.; Innocenti, M.; Yang, R.; Sun, F.; Jiang, Z.; Vizza, F. Heat treated carbon supported iron(ii)phthalocyanine oxygen reduction catalysts: elucidation of the structure−activity relationship using X-ray absorption spectroscopy. *Phys. Chem. Chem. Phys.* **2016**, *18*, 33142−33151.
(35) Chung, H. T.; Cullen, D. A.; Higgins, D.; Sneed, B. T.; Holby, E. F.; More, K. L.; Zelenay, P. Direct atomic-level insight into the active sites of a high-performance PGM-free ORR catalyst. *Science* **2017**, *357*, 479−484.
(36) Li, J.; Chen, M.; Cullen, D. A.; Hwang, S.; Wang, M.; Li, B.; Liu, K.; Karakalos, S.; Lucero, M.; Zhang, H.; Lei, C.; Xu, H.; Sterbinsky, G. E.; Feng, Z.; Su, D.; More, K. L.; Wang, G.; Wang, Z.; Wu, G. Atomically dispersed manganese catalysts for oxygen reduction in proton-exchange membrane fuel cells. *Nat. Catal.* **2018**, *1*, 935−945.
(37) Zitolo, A.; Goellner, V.; Armel, V.; Sougrati, M.-T.; Mineva, T.; Stievano, L.; Fonda, E.; Jaouen, F. Identification of catalytic sites for oxygen reduction in iron- and nitrogen-doped graphene materials. *Nat. Mater.* **2015**, *14*, 937−942.
(38) Johansson, L. Y.; Mrha, J.; Larsson, R. Elektrokatalyse der O2 reduktion in sauerer lösung mit hilfe der polymeren phthalocyanine. *Electrochim. Acta* **1973**, *18*, 255−258.
(39) Wang, X.; Wang, B.; Zhong, J.; Zhao, F.; Han, N.; Huang, W.; Zeng, M.; Fan, J.; Li, Y. Iron polyphthalocyanine sheathed multiwalled carbon nanotubes: A high-performance electrocatalyst for oxygen reduction reaction. *Nano Res.* **2016**, *9*, 1497−1506.
(40) Abel, M.; Clair, S.; Ourdjini, O.; Mossoyan, M.; Porte, L. Single Layer of Polymeric Fe-Phthalocyanine: An Organometallic Sheet on Metal and Thin Insulating Film. *J. Am. Chem. Soc.* **2011**, *133*, 1203−1205.
(41) Zhang, Z.; Yang, S.; Dou, M.; Liu, H.; Gu, L.; Wang, F. Systematic study of transition-metal (Fe, Co, Ni, Cu) phthalocyanines as electrocatalysts for oxygen reduction and their evaluation by DFT. *RSC Adv.* **2016**, *6*, 67049−67056.
(42) Zhang, H.; Zhang, S.; Wang, Y.; Si, J.; Chen, Y.; Zhuang, L.; Chen, S. Boosting the Performance of Iron-Phthalocyanine as Cathode Electrocatalyst for Alkaline Polymer Fuel Cells Through Edge-Closed Conjugation. *ACS Appl. Mater. Interfaces* **2018**, *10*, 28664−28671.
(43) Palusiak, M.; Rudolf, B.; Zakrzewski, J.; Pfitzner, A.; Zabel, M.; Grabowski, S. J. Intramolecular carbonyl···carbonyl interactions in W, Mo and Fe complexes containing the η1-N-maleimidato ligand: X-ray, DFT and AIM studies. *J. Organomet. Chem.* **2006**, *691*, 3232−3238.
(44) Yu, Y.-X. Binding Energy and Work Function of Organic Electrode Materials Phenanthraquinone, Pyromellitic Dianhydride and Their Derivatives Adsorbed on Graphene. *ACS Appl. Mater. Interfaces* **2014**, *6*, 16267−16275.
(45) McKeown, N. B. *Phthalocyanine Materials: Synthesis, Structure and Function*; Cambridge University Press, 1998.
(46) Kozlowski, C.; Sherwood, P. M. A. X-ray photoelectron-spectroscopic studies of carbon-fibre surfaces. Part 5.—The effect of pH on surface oxidation. *J. Chem. Soc., Faraday Trans. 1* **1985**, *81*, 2745−2756.
(47) Snezhkova, O.; Bischoff, F.; He, Y.; Wiengarten, A.; Chaudhary, S.; Johansson, N.; Schulte, K.; Knudsen, J.; Barth, J. V.; Seufert, K.; Auwärter, W.; Schnadt, J. Iron phthalocyanine on Cu(111): Coverage-dependent assembly and symmetry breaking, temperature-induced homocoupling, and modification of the adsorbate-surface interaction by annealing. *J. Chem. Phys.* **2016**, *144*, No. 094702.
(48) Lee, S. W.; Kim, B.-S.; Chen, S.; Shao-Horn, Y.; Hammond, P. T. Layer-by-Layer Assembly of All Carbon Nanotube Ultrathin Films for Electrochemical Applications. *J. Am. Chem. Soc.* **2009**, *131*, 671−679.

https://doi.org/10.1021/acscatal.2c00184
ACS Catal. 2022, 12, 7278−7287

(49) Tang, J.; Yang, J.; Zhou, X.; Xie, J.; Chen, G. Oxidation of acetylene black by nitric acid in hermetically sealed condition. *Microporous Mesoporous Mater.* **2014**, *193*, 54−60.
(50) Snezhkova, O.; Lüder, J.; Wiengarten, A.; Burema, S. R.; Bischoff, F.; He, Y.; Rusz, J.; Knudsen, J.; Bocquet, M.-L.; Seufert, K.; Barth, J. V.; Auwärter, W.; Brena, B.; Schnadt, J. Nature of the bias-dependent symmetry reduction of iron phthalocyanine on Cu(111). *Phys. Rev. B: Condens. Matter Mater. Phys.* **2015**, *92*, No. 075428.
(51) Wagner, C.; Naumkin, A.; Kraut-Vass, A.; Allison, J.; Powell, C., Jr; Rumble, J., X-ray photoelectron spectroscopy database, 20.(version 4.1). *Natl. Inst. Stand. Technol. NIST* **2012**.
(52) Greczynski, G.; Hultman, L. X-ray photoelectron spectroscopy: Towards reliable binding energy referencing. *Prog. Mater Sci.* **2020**, *107*, No. 100591.
(53) Hansch, C.; Leo, A.; Taft, R. A survey of Hammett substituent constants and resonance and field parameters. *Chem. Rev.* **1991**, *91*, 165−195.
(54) Kuznetsov, D. A.; Han, B.; Yu, Y.; Rao, R. R.; Hwang, J.; Román-Leshkov, Y.; Shao-Horn, Y. Tuning Redox Transitions via Inductive Effect in Metal Oxides and Complexes, and Implications in Oxygen Electrocatalysis. *Joule* **2018**, *2*, 225−244.
(55) Recio, F. J.; Cañete, P.; Tasca, F.; Linares-Flores, C.; Zagal, J. H. Tuning the Fe(II)/(I) formal potential of the FeN4 catalysts adsorbed on graphite electrodes to the reversible potential of the reaction for maximum activity: Hydrazine oxidation. *Electrochem. Commun.* **2013**, *30*, 34−37.
(56) Dutta, U.; Maiti, S.; Bhattacharya, T.; Maiti, D., Arene diversification through distal C (sp2)− H functionalization. *Science* **2021**, *372* DOI: 10.1126/science.abd5992.
(57) Touzalin, T.; Joiret, S.; Maisonhaute, E.; Lucas, I. T. Complex Electron Transfer Pathway at a Microelectrode Captured by in Situ Nanospectroscopy. *Anal. Chem.* **2017**, *89*, 8974−8980.
(58) Alsudairi, A.; Li, J.; Ramaswamy, N.; Mukerjee, S.; Abraham, K. M.; Jia, Q. Resolving the Iron Phthalocyanine Redox Transitions for ORR Catalysis in Aqueous Media. *J. Phys. Chem. Lett.* **2017**, *8*, 2881−2886.
(59) Wang, Y.; Yuan, H.; Li, Y.; Chen, Z. Two-dimensional iron-phthalocyanine (Fe-Pc) monolayer as a promising single-atom-catalyst for oxygen reduction reaction: a computational study. *Nanoscale* **2015**, *7*, 11633−11641.
(60) Chen, K.; Liu, K.; An, P.; Li, H.; Lin, Y.; Hu, J.; Jia, C.; Fu, J.; Li, H.; Liu, H.; Lin, Z.; Li, W.; Li, J.; Lu, Y.-R.; Chan, T.-S.; Zhang, N.; Liu, M. Iron phthalocyanine with coordination induced electronic localization to boost oxygen reduction reaction. *Nat. Commun.* **2020**, *11*, No. 4173.
(61) Wei, C.; Rao, R. R.; Peng, J.; Huang, B.; Stephens, I. E. L.; Risch, M.; Xu, Z. J.; Shao-Horn, Y. Recommended Practices and Benchmark Activity for Hydrogen and Oxygen Electrocatalysis in Water Splitting and Fuel Cells. *Adv. Mater.* **2019**, *31*, No. 1806296.
(62) Chen, J. G.; Jones, C. W.; Linic, S.; Stamenkovic, V. R. Best Practices in Pursuit of Topics in Heterogeneous Electrocatalysis. *ACS Catal.* **2017**, *7*, 6392−6393.
(63) Bonakdarpour, A.; Lefevre, M.; Yang, R.; Jaouen, F.; Dahn, T.; Dodelet, J.-P.; Dahn, J. Impact of loading in RRDE experiments on Fe−N−C catalysts: two-or four-electron oxygen reduction? *Electrochem. Solid-State Lett.* **2008**, *11*, B105.
(64) Jaouen, F.; Dodelet, J.-P. O2 Reduction Mechanism on Non-Noble Metal Catalysts for PEM Fuel Cells. Part I: Experimental Rates of O2 Electroreduction, H2O2 Electroreduction, and H2O2 Disproportionation. *J. Phys. Chem. C* **2009**, *113*, 15422−15432.
(65) Ke, K.; Hatanaka, T.; Morimoto, Y. Reconsideration of the quantitative characterization of the reaction intermediate on electrocatalysts by a rotating ring-disk electrode: The intrinsic yield of H2O2 on Pt/C. *Electrochim. Acta* **2011**, *56*, 2098−2104.
(66) Choi, C. H.; Lim, H.-K.; Chung, M. W.; Chon, G.; Ranjbar Sahraie, N.; Altin, A.; Sougrati, M.-T.; Stievano, L.; Oh, H. S.; Park, E. S.; Luo, F.; Strasser, P.; Dražić, G.; Mayrhofer, K. J. J.; Kim, H.; Jaouen, F. The Achilles' heel of iron-based catalysts during oxygen reduction in an acidic medium. *Energy Environ. Sci.* **2018**, *11*, 3176−3182.
(67) Li, J.; Sougrati, M. T.; Zitolo, A.; Ablett, J. M.; Oğuz, I. C.; Mineva, T.; Matanovic, I.; Atanassov, P.; Huang, Y.; Zenyuk, I.; Di Cicco, A.; Kumar, K.; Dubau, L.; Maillard, F.; Dražić, G.; Jaouen, F. Identification of durable and non-durable FeNx sites in Fe−N−C materials for proton exchange membrane fuel cells. *Nat. Catal.* **2021**, *4*, 10−19.
(68) Choi, C. H.; Baldizzone, C.; Polymeros, G.; Pizzutilo, E.; Kasian, O.; Schuppert, A. K.; Ranjbar Sahraie, N.; Sougrati, M.-T.; Mayrhofer, K. J. J.; Jaouen, F. Minimizing Operando Demetallation of Fe-N-C Electrocatalysts in Acidic Medium. *ACS Catal.* **2016**, *6*, 3136−3146.
(69) Kumar, K.; Asset, T.; Li, X.; Liu, Y.; Yan, X.; Chen, Y.; Mermoux, M.; Pan, X.; Atanassov, P.; Maillard, F.; Dubau, L. Fe−N−C Electrocatalysts' Durability: Effects of Single Atoms' Mobility and Clustering. *ACS Catal.* **2021**, *11*, 484−494.
(70) Kumar, K.; Dubau, L.; Mermoux, M.; Li, J.; Zitolo, A.; Nelayah, J.; Jaouen, F.; Maillard, F. On the Influence of Oxygen on the Degradation of Fe-N-C Catalysts. *Angew. Chem., Int. Ed.* **2020**, *59*, 3235−3243.

https://doi.org/10.1021/acscatal.2c00184
ACS Catal. 2022, 12, 7278−7287